Document donwnloaded from:

[http://redivia.gva.es/handle/20.500.11939/6094]

This paper must be cited as:

[Salcedo, R., Vallet, A., Granell, R., Garcera, C., Molto, E., Chueca, P. (2017). Eulerian-lagrangian model of the behaviour of droplets produced by an air-assisted sprayer in a citrus orchard. Biosystems Engineering, 154, 76-91.]

ivia
Institut Valencià
d'Investigacions Agràries

The final publication is available at

[https://doi.org/10.1016/j.biosystemseng.2016.09.001]

Copyright [Elsevier]

*Manuscript
Click here to download Manuscript: 160901_ Manuscript_def.docx Click here to view linked References

Patricia Chueca

Instituto Valenciano de Investigaciones Agrarias.

Centro de Agroingeniería.

Ctra. Moncada-Náquera km. 4.5-E-46113-Moncada, Valencia (Spain)

e-mail: chueca_pat@gva.es

Tel: +34 963424000

Fax: +34 963424001

EULERIAN-LAGRANGIAN MODEL OF THE BEHAVIOUR OF DROPLETS PRODUCED BY AN AIR-ASSISTED SPRAYER IN A CITRUS ORCHARD

R. SALCEDO [a], A. VALLET [b], R. GRANELL [a], C. GARCERÁ [a], E. MOLTÓ [a], P. CHUECA [a,*]

[a] Centro de Agroingeniería, Instituto Valenciano de Investigaciones Agrarias. CV-315 km. 10,7 46113 Moncada (Spain);

[b] Institut de Recherche en Sciences et Technologies pour l'Environnement et l'Agriculture, 361 rue JF Breton - 34 196 Montpellier (France)

[*]**Corresponding author**

E-mail address: chueca_pat@gva.es

Abstract

During pesticide applications to citrus trees using air-assisted (airblast) sprayers, only a proportion of the volume emitted reaches the vegetation and the rest is lost through drift, evaporation, etc. These losses can be hazardous for the environment. Knowing the characteristics of droplets within the turbulent currents around the canopy could improve the application efficiency. In a previous study, a 2D computational fluid dynamics (CFD) model was used to simulate the effect of a citrus canopy on the airflow from an air-assisted sprayer was developed and validated. It considered the first element of the tree canopy as a solid body instead of a porous one. The aim of this study was to analyse the behaviour of the droplets for pesticide applications on citrus by means of an Eulerian-Lagrangian CFD model. It simulated both the air current from the sprayer fan and the wind and the behaviour of the droplets sprayed. Distance, height, velocity, Reynolds number, temperature, geometric and volumetric diameters at different times were obtained. With these parameters, new variables related to the kinetics and evaporation droplets were calculated. Simulation results estimated that 44% of the total sprayed volume reached the target tree, 28% reached adjacent trees, 20% was deposited on the ground and 8% was lost as atmospheric drift. The results largely matched an experimental mass balance carried out under similar conditions. The proposed model appears to be an appropriate tool for simulating treatments with air-assisted sprayers operating in citrus orchards.

Key words: plant protection treatments, efficiency, simulation, CFD

Nomenclature table

Symbol	Name	Units
A	Constant	Dimensionless
B	Constant	Dimensionless
C	Constant	Dimensionless
D	Geometric diameter	µm
Dv	Volume diameter	µm
D_c	Distinctive diameter	µm
D_0	Initial droplet diameter	µm
E	Total kinetic energy	J
F_d	Drag force	N
g	Gravitational acceleration	m s^{-2}
I	Turbulence intensity	Dimensionless
k_0	Evaporation rate	μm^2 s^{-1}
M	Droplet mass	Kg
m_i	Droplet mass for a particle i	Kg
N	Size distribution	Dimensionless
n'	New size distribution	Dimensionless
P	Linear momentum magnitude	kg m s^{-1}
P_y	Horizontal linear momentum	kg m s^{-1}
P_z	Vertical linear momentum	kg m s^{-1}
Q	Nozzle nominal flow	l min^{-1}
q_0	Variable	μm^2 s^{-1} K^{-1}

q_1	Variable	μm^{-1}
Re	Reynolds number	Dimensionless
S	Nozzle section area	m^2
t_{life}	Droplet lifetime	S
U_d	Droplet velocity magnitude	m s^{-1}
U_{d_i}	Droplet velocity magnitude for a particle *i*	m s^{-1}
U_{dy}	Horizontal droplet velocity	m s^{-1}
U_{dy_i}	Horizontal droplet velocity for a particle *i*	m s^{-1}
U_{dz}	Vertical droplet velocity	m s^{-1}
U_{dz_i}	Vertical droplet velocity for a particle *i*	m s^{-1}
U_{fy}	Horizontal air fan velocity	m s^{-1}
U_{fz}	Vertical air fan velocity	m s^{-1}
U_m	Velocity magnitude of the cloud mass centre	m s^{-1}
U_{my}	Horizontal velocity of the cloud mass centre	m s^{-1}
U_{mz}	Vertical velocity of the cloud mass centre	m s^{-1}
u_{ref}	Reference velocity	m s^{-1}
U_s	Sedimentation velocity	m s^{-1}
u_z	Wind velocity	m s^{-1}
Y_d	Particle mass fraction	Dimensionless
Y_i	Horizontal coordinate for a particle *i*	m
Y_m	Horizontal coordinate of the cloud mass centre	m
z	Height	m
Z_i	Vertical coordinate for a particle *i*	m
Z_m	Vertical coordinate of the cloud mass centre	m
z_{ref}	Reference height	m
z_0	Roughness length	m
α	Nozzle angle	º
ΔT	Difference between wet bulb and dry bulb temperatures	ºC
ρ_a	Air density	kg m^{-3}
ρ_d	Water density	kg m^{-3}
μ_t/μ	Viscosity rate	Dimensionless
τ	Relaxation time	s
τ_s	Relaxation time at sedimentation	s

38

1. Introduction

Pesticide applications aim to place an optimal quantity of an active substance on the right part of the plant as safely and economically as possible. During the applications, only a part of the spray reaches the vegetation (Chen, Ozkan, Zhu, Derksen, Krause, 2013). The rest of the spray is lost to the ground or is dispersed into the atmosphere leaving the treated area (ISO, 2005) and evaporating. These losses may present a risk to human health and environment (Aktar, Sengupta, Chowdhury, 2009; Felsot et al., 2010; Mamane, Raherison, Tessier, Baldi, Bouvier, 2015).

The percentage of off-target losses determines the efficiency of applications. It depends on the design of the sprayer (Fox, Derksen, Zhu, Brazee, Svensson, 2008), its set up (Salyani, Miller, Farooq, Sweeb, 2013), the properties of the spray liquid (De Schampheleire et al., 2009), environmental conditions (Catania, Inglese, Pipitone, Vallone, 2011) and crop characteristics (SDTF, 1997).

Citrus are one of the most important crops in the world with a yearly production of 131 million tonnes. Spain is the sixth largest citrus producer and premier exporter of fresh citrus worldwide (FAO, 2012). In citrus orchards, pesticide applications are usually carried out using air-assisted (i.e. fan assisted) sprayers. The characteristics of the crop are very different to other crops such as vines, pear, etc. The main differences being that citrus trees are globular and have a very dense canopy throughout the whole year.

The efficiency of the applications has been assessed in field conditions measuring off-target losses, or by deposition or by mass balance (Balsari, Marucco, Tamagnone, 2005; ISO, 2005, Gil, Sinfort, Brunet, Polveche, Bonicelli, 2007; Salyani, Farooq, Sweeb, 2007; Chueca, Moltó, Garcerá, 2011). In citrus, the losses had been quantified between 18-50% (Salyani, Farooq, Sweeb, 2007; Chueca, Moltó, Garcerá, 2011). However, in these studies, it is very difficult to control all the factors that influence efficiency, and it is also almost impossible to reproduce them. They do not allow the detection of spatial irregularities in the spray plume because measurements are limited by the number and the situation of samplers. Also, such experiments are time-consuming and expensive both on human and financial resources.

Mathematical and computational tools enable development of spray models. They are a good alternative for or may complement field trials. There are a number of different approaches which have been taken including physics based-models taking into account the crop features, plume dispersion models, Lagrangian models and computational fluid dynamics (CFD) simulations. Models have been developed that are appropriate for different applications, e.g. spray penetration and deposition on the canopies (Larbi & Salyani, 2012ab), dispersion of pesticides in the atmospheric boundary layer (Bache & Sayer, 1975; Thompson & Ley, 1983; Steinke & Yates, 1989), spray drift near the sprayed area, aerial spraying (Teske et al., 2002; Tsai et al., 2005), and boom sprayers (Miller & Hadfield, 1989; Hobson, Miller, Walklate, Tuck, Western, 1993; Holterman, Van de Zande, Porskamp, Huijsmans, 1997; Lebeau, Verstraete, Schiffers, Destain, 2009),etc) (Butler Ellis & Miller, 2010).

CFD models allow analysis turbulent airflows produced by air-assisted sprayers. Moreover, they permit analysis of two-phase flows. For that purpose, CFD models integrate Lagrangian models that study the trajectory of sprayed droplets and these combination models are known as Eulerian-Lagrangian models. They allow the

inclusion of several parameters that are extremely hard to control during field experiments, such as sprayer setup (García Ramos et al., 2015), weather conditions (Reichard, Zhu, Fox, Brazee, 1992) and vegetation structure (Endalew et al., 2009).

Eulerian-Lagrangian CFD models have been developed to study the spray dispersion near the air-assisted sprayer (Xu, Walklate, Rigby, Richardson, 1998), the distance reached by droplets of a single nozzle (Zhu, Reichard, Fox, Brazee, Ozkan, 1994) and spray deposition on the leaves of grape vines (Da Silva, Sinfort, Tinet, Pierrat, Huberson, 2006) and pear trees (Endalew et al., 2010; Duga et al., 2013).

The present work is part of a project whose final purpose is to provide knowledge of the behaviour of sprayed droplets from an air-assisted sprayer in a citrus crop at orchard level, not the detailed behaviour of the spray inside the canopy or in the surroundings of the sprayer. As a first step, the behaviour of the airflow in citrus orchards was experimentally analysed and described. Two vortices were found, one behind and another over the target canopy (Fig. 1) (Salcedo, Garcerá, Granell, Moltó, Chueca, 2015a). As far as authors knowledge, these turbulent structures have not been previously described in any other fruit orchard or vineyard with less dense canopies. The next step was to develop a Eulerian 2D CFD model to reproduce the observed behaviour of the airflow beyond the target tree (Salcedo et al., 2015b) and it was validated. The phenomenon to be simulated is so complex that it was decided to begin the simulation process with a 2D model.

The objective of the present work was to develop a Lagrangian spray model and integrate it with the 2D Eulerian airflow model to reproduce pesticide applications in citrus with air-assisted sprayers under Mediterranean conditions at orchard level. This model was used to predict the fate of the sprayed droplets and these predictions were used to estimate a mass balance for the pesticide applications.

2. Material and Methods

2.1 Eulerian-Lagrangian model

Air and droplet spray movement modelling was performed using the CFD code ANSYS Fluent (ANSYS, Inc. Canonsburg, PA, USA).

2.1.1 2D Eulerian model overview

The 2D Eulerian model developed by Salcedo et al. (2015b) was used as a basis for this work. The domain height of the model was modified from 8 m to 13 m to expand the study area (Fig. 2). The edges A and B simulated the incoming air generated by an air-assisted sprayer. These edges were divided in 0.2 m sections, except for the first 0.4 m tall vertical section of edge A. The velocity and turbulence intensity assigned to each section were determined from field conditions (Salcedo et al., 2015b) (Table 1). The lower edge represented the ground, and the upper and the D edges were modelled as air outlets.

Inside the domain, three regions corresponding to the structure of the orchard were defined, each one representing the cross-section of a row of trees. The region nearest to the air inlet was modelled as a solid medium with homogeneous characteristics, while the other two regions were modelled as a porous media at the outside of the tree canopy with an open space in the centre. This is because the resistance offered

by the first tree is much higher compared to the other trees. In field experiments it was the first tree that produced vortices (Salcedo et al., 2015a) which are somewhat similar to those observed when wind approaches a building (i.e. a bluff body) (Oke, 1988). Because the first region was considered as a solid medium, its dimensions had to be smaller than the physical dimensions of the trees because otherwise the airflow would be more vertical and have a higher speed than found in the results of the field experiments. The tree characteristics assumed here were based on the results of previous studies in order to fit the simulation to the experimental data (Salcedo et al., 2012, 2013, 2015b).

The RANS (Reynolds Average Navier-Stokes) approximation was used for the simulation of airflow generated by the fan using a turbulence model SST k-ω (Menter, 1994). The computational domain was discretised by means of a finite volume method (Versteeg & Malalasekera, 1995). The spatial discretisation, including momentum and turbulent parameters, followed a second order upwind scheme. In this approach, higher-order accuracy is achieved at cell faces through a Taylor series expansion of the cell-centred solution about the cell centroid. The treatment of the pressure-velocity coupling was carried out by means of the SIMPLE algorithm (Ferziger & Peric, 2001). The convergence criteria chosen for the simulation was to obtain a minimum normalised residual value of 10^{-4} for all the parameters.

2.1.2 General considerations of the simulations

Due to the fact that the model was developed in 2D, simulations in this work were divided in two parts to consider the advance speed of the sprayer. An advance velocity of 1.65 km h^{-1} was assumed because this is the recommended value for applications against pests of citrus in Spain. At initial time (t = 0 s) it was considered that the central part of the fan outlet was in the plane represented in the model. Taking into account the advance speed and the width of fan airflow outlet of the sprayer (0.30 m), the time that the machine would take to move 0.15 m would be 0.35 s. For this reason, the first part of the simulation gathered information from the initial time (t = 0 s) to t = 0.35 s. This part (Part 1) simulates the movement of the equipment while spraying. During this part, atmospheric wind was not considered because the greater order of magnitude of the airflow generated by the fan. This consideration was based on preliminary simulations, where it was concluded that the influence of wind was negligible due to the high airflow velocity produced by the fan.

The second part (Part 2) of the simulation started immediately after t = 0.35 s and finished only when droplets were either deposited, evaporated or had left the computational domain. In this part, only atmospheric wind was considered. Consequently, C edge played two roles (Fig. 2): In the first instance, it was an air outlet but subsequently it represented the inlet for environmental airflow.

2.1.3 Droplet considerations

Although it is acknowledged that the prediction accuracy of Lagrangian models depends on the number of particles injected (Graham & Moyeed, 2002), in the simulations it was decided to introduce 1,500 droplets at t = 0 s. This value was considered sufficient for the purposes of the study and it represented a compromise between having a large number of droplets and the computational cost of simulation.

Droplet characteristics at the inlet (size, velocity, inlet point and angle) were based on experimental results (Chueca et al., 2011). The inlet point of droplets was defined on the basis of the equipment situation regarding A and B edges and the orientation of each nozzle in relation to the horizontal line during the experiment (Fig. 3i). The central axis of the droplet cone of each nozzle defined the inlet points of the droplets. Therefore, droplets were introduced through sections between 0.6 and 1.8m up from edge A (from A80 to A180) (Fig. 3ii). Droplets were uniformly distributed in each section of the model (250 droplets per section).

Droplet size and velocity were based on the characteristics of droplets from full-cone disc-core nozzle (Model D3 DC35, TeeJet, Spraying Systems Co., Wheaton, IL, USA). This type of nozzle is one of the standard nozzles that is widely used in pesticide applications in citrus in Spain.

Droplet inlet velocity U_d (m s^{-1}) was the estimated initial velocity in the nozzle. This value was calculated by dividing the nozzle nominal flow at 1MPa, Q (2 l min^{-1} = $3.33 \cdot 10^{-5}$ m^3 s^{-1}), and the section area of the nozzle outlet, S (m^2). Horizontal U_{dy} and vertical U_{dz} velocity components for each section were calculated taking into account, the magnitude U_d and the orientation (α) of the corresponding nozzles to each section.

Droplets generated by the sprayer were considered as spherical water particles. The size distribution was assumed to follow the Rosin-Rammler distribution (Eq. 1) (Duga et al., 2013):

$$1 - Y_d = \exp\left(-\left(\frac{D}{D_c}\right)^n\right) \quad (1)$$

Where D (μm) is the droplet volume diameter, D_c is a distinctive diameter (μm) (in ANSYS Fluent code, it refers to it as the mean diameter), Y_d (-) is the particle mass fraction with a smaller diameter than D, and n (-) is the uniformity constant (in ANSYS Fluent code, it is referred to as the spread parameter). To fit the size of population of droplets injected in the simulation to the Rosin-Rammler distribution, Fluent requires the minimum, mean and maximum values of droplet diameter and the parameter n.

In this work, the minimum diameter was considered to be 1 μm and the mean diameter to be 350 μm which corresponded to the *Dv50* (personal communication with the nozzle manufacturer). The maximum diameter was considered to correspond to the *Dv90*. This value was estimated through Eq. 1 for Y_d = 90%, considering D_c = 350 μm and n = 3.5 (software default value), and the result was 444 μm.

To know the value of *n'* for the considered distribution (D_{min}= 1 μm, D_{mean}= 350 μm, D_{max}= 444 μm), a preliminary simulation using these data and n = 3.5 was carried out but stopped at 0.05 s, just when droplets left the inlets. The value of *Dv90'* for the resulting population was then calculated, having a value of 410 μm. With this value, the spread parameter (*n'*) was calculated through Eq. 1, for Y_d = 90%, D_c = 350 μm and D = 410 μm, and the result was *n'* = 5.3. A new preliminary simulation was then run with these data (D_{min}= 1 μm, D_{mean}= 350 μm, D_{max}= 444 μm, and *n'* = 5.3) but stopped at 0.05 s. No significant differences were found with the previous simulation and thus these values were adopted for the study.

The initial temperature of the droplets was considered to be 15ºC.

A stochastic monitoring was chosen to model turbulent particle distribution. A discrete

random walk model was selected in order to include the effect of instant fluctuations on sprayed droplet trajectories. Velocity fluctuation components were constant discrete functions of time intervals. The arbitrary value remained constant depending on characteristic life span of the vortices. Effects such as droplet breaking, evaporation or coalescence between two droplets were included because these are common phenomena affecting droplets during the atomisation processes (Ruger, Hohmann, Sommerfeld, Kohnen, 2000). This was done by enabling the corresponding options in the Fluent software.

2.1.4 Ambient air and atmospheric wind considerations

The ambient air within the domain was considered as an incompressible and isothermal fluid, with a Newtonian behaviour, composed of nitrogen, oxygen and water vapour. A mean air temperature of 22 ºC and a relative humidity of 59% was assumed, corresponding to the measured experimental values (Chueca et al., 2011).

The atmospheric wind airflow inlet was considered to be parallel to the ground, so the vertical component of the wind velocity was 0 m s^{-1} and the horizontal component of the wind was modelled using the process described below.

In general, wind speed increases with height above the ground up to the tree top and a smooth transition exists between the tree top and the wind profile over the canopies (Cionco, 1965; Bergen, 1971; Georgiadis, Dalpane, Rossi, Nerozzi, 1996; Teske, Thistle, Ice, 2003). Nevertheless, in this work it was decided to simplify the phenomenon, due to the low wind velocity considered in the model at 7 m height (1.01 m s^{-1}), based on field measurements (Chueca et al., 2011). For this reason, the perpendicular component of wind velocity between rows, below 3 m, was assumed to have a constant value of 0.1 m s^{-1} based on field measurements with u_{ref} 1.01 m s^{-1} at 7 m high (Eq. 2 for $z < 3$ m). Between 3 m height up to the top of the domain, air velocity u_z (m s^{-1}) at a height z (m) was defined through a logarithmic function based on the wind profile proposed by Arya (1988) (Eq. 2 for $z \geq 3$ m). The profile of wind velocities used during part 2 is shown at Fig. 4.

$$u_z = 0.1 \text{ m s}^{-1} \qquad z < 3 \text{ m}$$

$$u_z = u_{ref}\left[\frac{ln\left(\frac{z}{z_0}\right)}{ln\left(\frac{z_{ref}}{z_0}\right)}\right] \qquad z \geq 3 \text{ m} \tag{2}$$

Where:

- u_{ref} (m s^{-1}) is the reference velocity, measured at a reference height z_{ref} (m). In this work, u_{ref} was considered 1.01 m s^{-1} and z_{ref} 7 m (Chueca et al., 2011)
- z_0 (m) stands for roughness length of the ground, and the 0.001 m value was considered (Salcedo et al., 2015b). This value was defined considering the ground without obstacles (Davenport, Grimmond, Oke, Wieringa, 2000).

For the air inlet in the second part of the simulation, a turbulence intensity I (%) of 5% and a turbulent viscosity ratio $\mu_t/\mu = 10$ were adopted.

2.2 Analysis of droplet behaviour during simulation

For spray droplets analysis, droplet data were taken at different times (t = 0.10 s, t = 0.20 s, t = 0.35 s, t = 2.35 s, t = 5.35 s, t = 8.35 s, t = 11.35 s, and t = 17.35 s). These were chosen because differences in the spectra between them were considered significant.

At each time, the number of droplets in the different sub-domains (target vegetation, adjacent trees, ground and air) was calculated. The following considerations were taken into account for each sub-domain:

- Droplets deposited on the vegetation of the first tree (the target vegetation) corresponded to the droplets that stayed on the solid tree.
- For trees in rows 2 and 3 (adjacent trees), as they were porous bodies, droplets did not stay on them. Therefore, it was considered that droplets that reached the part of the ground under their canopies had been deposited in these trees.
- Ground losses were considered as droplets deposited on the ground and droplets that left the domain below 5 m height.
- Atmospheric drift was calculated as the portion of evaporated droplets and droplets that left the domain above 5 m height (Chueca et al., 2011).
- The remaining droplets in the domain which had not been deposited (on the trees or on the ground) or lost as atmospheric drift were considered to be still in the air.

The following parameters of each droplet were also measured: horizontal distance (m) to the coordinate origin (Fig. 2), distance to the ground (m), horizontal and vertical velocity components (U_{dy}, U_{dz}) (m s^{-1}), geometric diameter (µm), temperature (°C) and Reynolds number (-).

2.2.2. Dynamic behaviour of droplet cloud

For the analysis of the dynamic behaviour of droplet cloud the following parameters were calculated:

- Mass centre of the cloud of droplets for each moment (Eq. 3).

$$\begin{cases} Y_m = \frac{\sum Y_i m_i}{\sum m_i} \\ Z_m = \frac{\sum Z_i m_i}{\sum m_i} \end{cases} \quad (3)$$

Where (Y_m, Z_m) (m) are the horizontal and vertical coordinates of the mass centre, (Y_i, Z_i) (m) are the horizontal and vertical coordinates of each droplet and m_i (kg) is the mass of each droplet calculated from the diameter of each droplet and considering droplets with spherical shape.

- Velocity of mass centre (Eq. 4).

$$\begin{cases} U_{my} = \frac{\sum m_i U_{dy_i}}{\sum m_i} \\ U_{mz} = \frac{\sum m_i U_{dz_i}}{\sum m_i} \end{cases} \quad (4)$$

Where (U_{my}, U_{mz}) (m s^{-1}) are the horizontal and vertical components of the velocity of the mass centre and (U_{dy_i},U_{dz_i}) (m s^{-1}) are the horizontal and vertical components of the velocity of each droplet.

- Translational momentum or total linear momentum of the system (Eq. 5).

$$\begin{cases} P_y = \sum m_i U_{dy_i} \\ P_z = \sum m_i U_{dz_i} \end{cases} \quad (5)$$

Where (P_y, P_z) (kg m s^{-1}) are the horizontal and vertical components of the momentum

- Total kinetic energy (Eq. 6).

$$E = \sum \left(\frac{1}{2} m_i U_{d_i}^2 \right) \quad (6)$$

Where E (J) represents the system kinetic energy and U_{d_i} (m s^{-1}) is the magnitude of the velocity of each droplet.

2.2.3. Droplet kinetics and evaporation during treatment

In order to analyse droplet kinetics and evaporation during treatment, the set of physical parameters proposed by Holterman (2003) was calculated for the times corresponding to the second part of the simulation. For these calculations, droplets exposed to the wind action were only considered, that is, droplets above at least 3.0 m height.

i) <u>Droplet kinetics</u>

- The drag coefficient of each droplet C_d (-) was calculated (Eq. 7) (Holterman, 2003).

$$C_d = \left(\left(\frac{a}{Re} \right)^c + b^c \right)^{1/c} \quad (7)$$

Where a, b and c are constants, with values of 24, 0.32 and 0.52 respectively, and Re is the Reynolds number (-). To calculate Re, Fluent uses the velocity of droplet relative to ambient air, which is the difference between the droplet velocity and the air velocity (Eq. 8).

$$Re = \frac{\rho_a D U_d}{\eta_a} \quad (8)$$

Where ρ_a (kg m^{-3}) is the air density, D (m) is the diameter of the droplet, U_d (m s^{-1}) is its velocity relative to the air stream, and η_a (kg m^{-1} s^{-1}) is the dynamic viscosity of air.

- Relaxation time τ (s) was calculated (Eq. 9), which is the time that droplets need to adapt to local changes in air velocity.

$$\tau = \frac{4 \rho_d D}{3 \rho_a U_d C_d} \quad (9)$$

Where ρ_d (kg m^{-3}) is the water density, D (m) is the droplet diameter, ρ_a (kg m^{-3}) is the air density, U_d (m s^{-1}) is the velocity of the droplet and C_d (-) is the drag coefficient of each droplet.

- Drag force F_d (N) can be calculated from relaxation time (Eq. 10):

$$F_d = \frac{mU_d}{\tau} \quad (10)$$

Where m (kg) is the mass of the droplet, U_d (m s^{-1}) is the velocity of the droplet and τ (s) is the relaxation time of each droplet.

In a laminar flow regime, drag force F_d and gravity force are the major forces that act on droplets. When droplets descend at a constant rate they descend at sedimentation velocity U_s (m s^{-1}). In order to estimate the value of U_s for each droplet, an algorithm relating U_s and D was used (Eq. 11) (Holterman, 2003).

$$\begin{cases} U_s = 4066.5D - 0.0655 & D \geq 150\mu m \\ U_s = 1 \cdot 10^7 D^{1.899} & D < 150\mu m \end{cases} \quad (11)$$

It is important to consider U_s because it is assumed that when it is < 10% of wind speed, droplets are become part of atmospheric drift (Holterman, 2003).
Relaxation time at sedimentation τ_s (s) was calculated using Eq. 13.

$$\tau_s = \frac{U_s}{g} \quad (13)$$

Where g is the gravitational acceleration (9.81 m s^{-2}).

Droplets size changes with time due to evaporative effects, affecting the calculated parameters. For this reason, mean values and the standard error of U_s, τ, τ_s and F_d were calculated for the different times from t = 0.35 s to t = 17.35 s (t = 0.35 s, t = 2.35 s, t = 5.35 s, t = 8.35 s, and t = 11.35 s).

In order to study droplet depositions, the relationship between the distance to the ground (height) and the parameters U_s and τ_s was analysed for each time. The mean values were calculated for each time, every 0.5 m between a height of 3 m and 7 m (above this height there were not droplets in the simulation).

ii) <u>Droplet evaporation</u>

In order to analyse the effects of evaporation, two parameters were calculated: the evaporation rate k_0 (μm^2 s^{-1}) (Eq. 14), which studied size variations over time, and the lifetime of evaporating droplets t_{life} (s) (Eq. 15), which estimates droplet life before complete evaporation.

$$k_0 = q_0 \Delta T (1 + q_1 D) \quad (14)$$

Where D is the droplet diameter (μm), ΔT (ºC) is the difference between wet bulb and dry bulb temperatures, and q_0 (μm^2 s^{-1} K^{-1}) and q_1 (μm^{-1}) variables are other two parameters depending on temperature and relative humidity. In this work, values of q_0 and q_1 estimated by Holterman (2003) for an ambient temperature of 20ºC and a relative wind humidity of 50% were used because these conditions are similar to our experimental conditions (22.3ºC and 58.71%).

To study the evaporative effect on droplets over time, the evaporation rate was calculated for each moment and every 0.5 m between 3 m and 7 m height. The mean size of the droplets for each height and wind mean velocity was also calculated.

The equation used to determine t_{life} was:

$$t_{life} = \frac{2}{q_0 q_1^2 \Delta T}(q_1 D_0 - \ln(1 + q_1 D_0)) \quad (15)$$

Where D_0 (μm) is the initial droplet diameter. In this work, D_0 was considered as the droplet diameter at t = 0.35 s, which is the time in which droplets are exposed to wind.

Based on the results of t_{life}, the number of potentially evaporated droplets at the end of the simulation (t = 17.35 s) was calculated. This number was compared with the number of total evaporated droplets according to the results of the simulation.

2.2.4. Mass balance and experimental data comparison

The cumulated number of droplets deposited on vegetation (target and adjacent trees), ground losses and atmospheric drift was estimated at the end of the simulation period.

From these data, and taking into account the 1,500 droplets introduced in the simulation, the percentage of droplets ending up in each sub-domain when the simulation was complete was calculated.

Because droplet size decreases with time, different droplet sizes predominate in the deposit on each sub-domain. For example, droplets in the target vegetation were coarser than the droplets lost by drift. Therefore, the percentage of the total sprayed volume corresponding to the droplets on each sub-domain was different to the percentage of droplets in each location. For this reason, the mass balance at the end of the simulation as the percentage of volume deposited on each sub-domain respect to the initial spray volume applied was calculated. The initial spray volume was calculated as the sum of the initial mass of the 1,500 droplets. At the end of the simulation, the spray volume deposited in each sub-domain was provided by Fluent.

The results of mass balance were compared to experimental results (Chueca et al., 2011).

3. Results and Discussion

3.1 General description of the cloud movement.

Droplet movement during Part 1, when the inlet airflow into the domain was produced by the fan is shown in Figs. 5 and that when the inlet airflow was produced by wind (Part 2) is shown in Fig.6.

The spray plume initially split into two clouds because the airflow generated by the fan bifurcated when it reached the first (solid) tree. One cloud, hereafter called Cloud 1, passed below the first tree, and the other over the canopy and was designated Cloud 2 (Fig. 5i).

Cloud 1 was formed by the droplets introduced through section A80. They were then trapped in the accelerating airflow that occurred between the ground and the solid tree. Cloud 2 was formed by droplets introduced into sections A140, A180 and 50 droplets from A120. The rest of spray plume was directed towards the target tree and deposited there.

Cloud 1 travelled horizontally until 9 m, where the second tree was located. The height of its mass centre decreased from around 0.7 m to 0.1 m (Table 2 and Table 3). The second tree, whose body was porous, produced a velocity gradient that affected each droplet and modified the shape of Cloud 1. Spray in this cloud mainly deposited on the ground and on the second tree although some of them evaporated. At 5.35 s no droplets from Cloud 1 were found in the simulation (Fig. 6ii).

During Part 1 when the airflow was produced by the fan, Cloud 2 followed the profile of the velocity of the airflow generated by the fan and droplets moved en masse. Cloud 2 showed an important vertical movement reaching a maximum height of 7 m at 0.35 s (Fig. 9ii). During Part 1 the centre of mass of Cloud 2 moved from 3 m to 4.9 m.

When the fan was not used to provide airflow in the model (Part 2), Cloud 2 became more dispersed and it started to lose height. It then descended and moved horizontally due to the influence of wind because a vertical airflow component was not included. Some spray was deposited in the second tree (between 2.35 s and 5.35 s) and in the third tree (between 8.32 and 17.35 s) (Fig. 6) and the remaining droplets fell to the ground between the trees, evaporated or left the computational domain.

3.2 Droplet size and velocity, total linear momentum and total kinetic energy.

The geometric and volumetric diameters of droplets are shown in Fig. 12 and Fig. 13 respectively. Figure 10 shows the velocity magnitude of droplets and values of the velocity of the centre of mass of the spray cloud are shown in Table 2 and Table 3

In Cloud 1, droplet size decreased quickly with time. Airborne droplets became more homogeneous at 2.35 s hence the geometric statistics (minimum, maximum and average - Fig. 12i) and the volumetric statistics (Dv10, Dv50 and Dv90 - Fig. 13i) began to converge. Because the blockage of the first tree caused an acceleration between the ground and the tree, droplet velocity increased between 0 s and 0.20 s (Table 1). After this time, droplet velocity decreased sharply (Table 2, Table 3 and Fig. 10i).

In Cloud 2, significant changes in droplet size were not observed until 2.35 s. From this time, droplet size decreased gradually (Fig. 12ii and Fig. 13iii). Droplet velocity decayed quickly from its introduction in the simulation until 2.35 s, after which, it reduced steadily (Table 2, Table 3 and Fig. 10ii).

Total linear momentum and the total kinetic energy of each of the clouds followed the trends observed by the velocity of the corresponding centre of mass (Table 2 and Table 3).

3.3 Reynolds number of droplets

In Part 1 of the simulation, both clouds presented similar behaviour in the evolution of the Reynolds number with time. Mean and maximum values of the Reynolds number decreased between 0.10 s and 0.20 s (Mean values: from 60 to 24 in cloud 1 and from 56 to 35 in cloud 2). However, the values increased to more than 100 at 0.35 s, showing a less laminar behaviour (Fig. 11). This could be explained in Cloud 1 by velocity variations when penetrating the porous body and in Cloud 2 because droplets had just travelled through the vortex that occurs above the first tree canopy (Fig. 5).

At 2.35 s, Reynolds number reduced; in Cloud 1 to a value of 1 and in Cloud 2 to16. During the rest of the simulation, the Reynolds number of Cloud 2 continued to slowly decrease to values < 1. The lack of airflow generated by the fan is the main reason for this decrease. With only wind causing air movement, droplets lost their inertia and their behaviour was governed by the viscous drag of air.

3.4 Droplet kinetics and evaporation

Sedimentation velocity magnitude (U_s) decreased with time (Table 4) because droplet diameters decreased gradually due to evaporation. Also, U_s decreased with height (Table 5) because of the reduced size of the droplets at greater heights, and because droplet velocity reduced with time. According to Holterman (2003), when droplets have an $U_s <$ 10% of the wind velocity, they are susceptible to being transported by the airflow and becoming atmospheric drift. Therefore, in the simulation, droplets susceptible to becoming drift occur a lower height with time for example, at 0.35 s susceptible droplets were found at heights between 6.5 and 7.0 m but at 8.35 s droplets they occurred at heights between 4.5 and 6 m.

Values of τ_s were higher than τ, therefore, droplets required more time to adapt to changes in airflow during sedimentation. Both τ_s and τ decreased with time (Table 4). Droplets required less time to adapt to changes in airflow as the simulation advanced. This would fit in with the idea that droplets lose inertia over time.

The value of τ_s decreased with height (Table 6) according to the trend shown by U_s. Therefore, the time droplets needed to reach sedimentation velocity was shorter as droplets reached greater height.

The values of k_o generally decreased with height and with time (Table 7). This was related to the fact that the range of droplet sizes decreased and the spray clouds became more homogeneous with time.

Based on the estimated t_{life} from 0.35s (Eq. 15), at 20 s the number of droplets that would have evaporated was 281. In the simulation, between 0.35 s and 20.35 s the number of evaporated droplets was 260, which was considered to be a good approximation.

3.5 Mass balance and experimental data comparison

The evolution of number of droplets found in each sub-domain with time is shown in Fig. 7.

At 0.35 s, with the presence of air movement from the fan, 31% of the total droplets were deposited on the first canopy. Cloud 1 was made up of 16% of the droplets and Cloud 2 was formed by 51 % of the droplets. The remaining 2% of droplets had evaporated.

At 2.35 s, with the presence of wind, only 45% of the initial droplets remained in the simulation (3% in cloud 1 and 42% in cloud 2). Accumulated droplets in the first tree were 33% and in the second tree 11%. 10% of droplets had evaporated and 1% were deposited on the ground.

At 8.35 s, only 16% of the initial droplets remained in the computational domain. The

484 percentage of droplets retained in the second and third canopies increased to 25%,
485 evaporated droplets to 19% and deposited on the ground to 7%.

486 At 11.35 s, only 7% of the droplets remained in the air. Eighty droplets (5%) had left the
487 domain, pushed by the wind, 15 of them above 5.0 meters. Droplets on adjacent
488 vegetation accounted for 26%, 19% had evaporated and 10% were located on the
489 ground.

490 The final results of the simulation estimated that 33% of the droplets were deposited on
491 the first tree, 29% of the droplets were deposited between the second and the third tree,
492 22% of the droplets evaporated or abandoned the domain above 5.0 m and 16% of the
493 droplets were deposited on the ground or they escaped from the domain below 5.0 m.

494 Mean droplet size decreased with time, therefore different droplet sizes predominated in
495 each sub-domain. For example, droplets in the target vegetation were larger in diameter
496 than droplets lost by drift. Therefore, the percentage of the total sprayed volume
497 corresponding to the droplets on each sub domain was different to the percentage of
498 droplets in each location. In this way, the percentage of the total sprayed volume
499 deposited on the target tree was 44%, 28% was deposited on the adjacent vegetation,
500 20% on the ground and 8% was lost as drift.

501 Comparing these results with those obtained in field experiments by Chueca et al.
502 (2011) it is observed that the mean deposition achieved over target trees was similar,
503 44% versus 43% respectively (Table 8).

504 The deposition over the trees in the adjacent swaths was 28% in the model compared to
505 5% in the experiment. This difference could be due to the fact that in the model, wind
506 direction was perpendicular to the trees, and in the field experiment, wind direction
507 varied between replicates. Another reason could be that Cloud 1 in the simulation
508 arrived immediately at the second tree though a gap between the first tree and the
509 ground but in the field experiment trees were planted over raised beds (200 mm high, 2
510 m wide at the top and 3 m wide in the base) that may affect the droplet trajectory.

511 The total quantity of losses over the ground during the experiments was 25% as
512 opposed to 20% in the simulation.

513 Experimental drift accounted for 18% compared to 8% estimated by the model. In the
514 experimental assay, losses from evaporation could not be assessed. Trajectories obtained
515 by the simulation reflected that many droplets found at heights over 5.0 m, started to
516 descend after the second or third tree or directly to the ground. However, in the field
517 experiment spray sampled at 5 m height was considered drift without taking into
518 account that a proportion might be descending and heading for adjacent trees or the
519 ground.

520 Finally, it is worthwhile noting that the field experiment could not account for the
521 location of 9% of the sprayed volume.

522 **4. Conclusions**

523 A 2D Eulerian-Lagrangian CFD model was developed to reproduce pesticide treatments
524 with air-assisted sprayers on citrus at orchard level. In general, the results obtained with
525 the simulation were comparable to those obtained in field conditions. Consequently, the

model could be considered an appropriate tool for estimating the mass balance of spray applications on citrus and therefore their efficiency. It may also serve to study the effect of different factors affecting the efficiency like temperature and relative air humidity, the turbulence intensity of wind, physicochemical properties of the spray mix, type and orientation of nozzles and tractor advance speed.

Improvements to the model and further analysis should include:

- Improving the model approach by carrying out sensitivity analysis of the inputs such as the number, and initial temperature of droplets, the characteristics of trees (porosity, shape and size) and the roughness of ground; including a smooth transition in the atmospheric wind profile over the vegetation (Teske, Thistle, Ice, 2003).
- Validate the model with further experimental data
- Designing a 3D Eulearian-Lagrangian model based on the 2D model.

Acknowledgments

This work was partially financed by the Spanish Ministry of Economy (projects AGL2007-66093-C04-01 and AGL2010-22304-C04-01) and the European Regional Development Fund (ERDF). Ramon Salcedo is recipient of a postgraduate FPI-INIA scholarship. Particular thanks to Fernando Perez and Alejandro Escario for their help.

References

Aktar, M.W., Sengupta, D., & Chowdhury, A. (2009). Impact of pesticides use in agriculture: their benefits and hazards. *Interdisciplinary Toxicology*, 2, 1-12.

Arya, S. P. (1988). Introduction to micrometeorology. *Academic Press*, San Diego.

Bache, D.H., & Sayer, W.J.D. (1975). Transport of aerial spray, I. A model of aerial dispersion. *Agricultural Meteorology*, 15, 257-271.

Balsari, P., Marucco, P., & Tamagnone M. (2005) A system to assess the mass balance of spray applied to tree crops. *Transactions of the ASAE*. 48, 1689-1694.

Bergen, J. D. (1971). Vertical profiles of wind speed in a pine stand. *Forest Science* 17(3), 314-321.

Butler Ellis, M.C., & Miller, P.C.H. (2010). The Silsoe Spray Drift Model: A model of spray drift for the assessment of non-target exposures to pesticides. *Biosystems Engineering*, 107, 169-177.

Catania, P., Inglese, P., Pipitone, F. & Vallone, M. (2011) Assessment of the wind influence on spray application using an artificial vineyard. *European Journal of*

Horticultural Science, 76, 102-108.

Chen, Y., Ozkan, E., Zhu, H., Derksen, R. & Krause, CR. (2013) Spray deposition inside tree canopies from a newly developed variable-rate air-assisted sprayer. *Transactions of ASABE*, 56(6), 1263-1272.

Chueca, P., Moltó, E., & Garcerá, C., (2011). Influence of nozzles on mass balance of spray applications in citrus. In: Centre Ctifl Lanxade. *Proceedings of 11th Workshop. Sustainable Plant Protection Techniques in Fruit Growing (Suprofruit 2011)*. Bergerac, France. p. 8-10.

Cionco, R. M. (1965). A mathematical model for air flow in a vegetative canopy. *Journal of Applied Meteorology*, 4, 517-522.

Da Silva, A., Sinfort, C., Tinet, C., Pierrat, D., & Huberson, S. (2006). A Lagrangian model for spray behaviour within vine canopies. *Journal of Aerosol Science*, 37, 658-674.

Davenport, A.G., Grimmond, C.S.B., Oke, T.R., & Wieringa J. (2000). Estimating the roughness of cities and sheltered country. *Proceedings of 12th American Meteorology Society Symposium on Applied Climatology*, Asheville, NC, 96–99.

De Schampheleire, M., Nuyttens, D., Baetens, K., Cornelism W., Gabriels, D., & Spanoghe, P. (2009). Effects on pesticide spray drift of the physicochemical properties of the spray liquid. *Precision Agriculture*, 10, 409-420.

Duga, A.T., Defraeye, T., Hendrickx, N., Dekeyser, D., Nuyttens, D., Nicolai, B., & Verboven, P. (2013). Sprayer-canopy characterization using field experiments and CFD modelling. In E. Moltó et al., (eds). Book of Abstracts. *12th International Workshop on Sustainable Plant Protection Techniques in Fruit Growing (SuproFruit2013)*. IVIA, Valencia, Spain. p. 100-102.

Endalew, A.M., Hertog, M., Gebrehiwot, M.G., Baelmans, M., Ramon, H., Nicolaï, B.M., & Verboven, P. (2009). Modelling airflow within model plant canopies using an integrated approach. *Computers & Electronics in Agriculture*, 66, 9-24.

Endalew, A.M., Debaer, C., Rutten, N., Vercammen, J., Delele, M.A., Ramon, H., Nicolaï, B.M., & Verboven, P. (2010). A new integrated CFD modelling approach towards air-assisted orchard spraying. Part II. Validation for different sprayer types. *Computers & Electronics in Agriculture*, 71, 137-147.

FAO (Food and Agriculture Organization of the United Nations), 2012. Agricultural commodities production. Available in http://faostat3.fao.org/faostat-gateway/go/to/browse/Q/*/E.

Felsot, A.S., Unsworth, J.B., Linders, J.B.H.J., Roberts, G., Rautman, D., Harris, C., & Carazo, E. (2010). Agrochemical spray drift; assessment and mitigation-A review. *Journal of Environmental Science and Health Part B*, 46, 1–23.

Ferziger, J.H., & Peric, M. (2001) *Computational Methods for Fluid Dynamics*. (3rd ed.). Berlin: Springer-Verlag, (Chapter 4). Available at https://docs.google.com/file/d/0B7WvmGcRs5CzanBEeDlDaEk3dEU/edit. (Accessed January 2015).

Fox, R. D., Derksen, R. C., Zhu, H., Brazee, R. D., & Svensson S. A. (2008). A history of air-blast sprayer development and future prospects. *Transactions of ASABE*, 51(2), 405-410.

García Ramos, F.J., Malón, H., Aguirre, A.J., Boné, A., Puyuelo, J., & Vidal, M. (2015). Validation of a cfd model by using 3D sonic anemometers to analyse the air velocity generated by an air-assisted sprayer equipped with two axial fans. *Sensors*, 15, 2399-2418.

Georgiadis, T., Dalpane, E., Rossi, F., & Nerozzi, F., 1996. Orchard atmosphere physical exchanges: modelling the canopy aerodynamics. *ISHS Acta Horticulturae*, 416, 177-182.

Gil, Y., Sinfort, C., Brunet, Y., Polveche, V., & Bonicelli, B. (2007) Atmospheric loss of pesticides above an artificial vineyard during air-assisted spraying. *Atmospheric Environment*, 41, 2945–2957.

Graham, D., & Moyeed, R. (2002). How many particles for my Lagrangian simulation? *Powder Technology*, 125, 179-186.

Hobson, P.A., Miller, P.C.H., Walklate, P.J., Tuck, C.R., & Western, N.M. (1993). Spray drift from hydraulic spray nozzles: the use of a computer simulation model to examine factors influencing drift. *Journal of Agricultural Engineering Research*, 54, 293-305.

Holterman, H.J., Van de Zande, J.C., Porskamp, H.A.J., & Huijsmans, J.F.M (1997). Modelling spray drift from boom sprayers. *Computers & Electronics in Agriculture*, 19,

1-22.

Holterman, H.J. (2003). Kinetics and evaporation of water drops in air. IMAG report 2003-12. Wageningen UR, Holland.

ISO TC 23/SC 06 N 22866. (2005). *Equipment for crop protection – methods for the field measurement of spray drift*.

Larbi, P. A., & Salyani, M. (2012a). Model to predict spray deposition in citrus airblast sprayer applications; part 1. Spray dispersion. *Transactions of the ASABE*, 55(1), 29-39.

Larbi, P. A., & Salyani, M. (2012b). Model to predict spray deposition in citrus airblast sprayer applications; part 2. Spray deposition. *Transactions of the ASABE*, 55(1), 41-48.

Lebeau, F., Verstraete, A., Schiffers, B., & Destain, M.F. (2009). Evaluation of realtime spray drift using RTDrift Gaussian advection-diffusion model. *Communications in Agricultural and Applied Biological Science*, 74, 11-24.

Mamane, A., Raherison, C., Tessier, J.F., Baldi, I., & Bouvier, G. (2015). Environmental exposure to pesticides and respiratory health. *European Respiratory Review*, 24, 462-473.

Menter, F.R. (1994). Two-Equation Eddy-Viscosity Turbulence Models for Engineering Applications. *AIAA Journal*, 32, 1598-1605.

Miller, P.C.H., & Hadfield, D.J. (1989). A simulation model of the spray drift from hydraulic nozzles. *Journal of Agricultural Engineering Research*, 42, 135-147.

Oke, T.R. (1988). Street design and urban canopy layer climate. Energy and Buildings, 11, 103–113.

Reichard, D.L., Zhu, H., Fox, R.D., & Brazee, R.D. (1992). Computer simulations of variables that influences spray drift. *Transactions of ASAE*, 35, 1401-1407.

Ruger, M., Hohmann, S., Sommerfeld, M., & Kohnen, G. (2000). Euler/Lagrange calculations of turbulent sprays: the effect of droplet collisions and coalescence. *Atomization and Sprays*, 10(1), 47-81.

683 Salcedo, R., Granell, R., Garcerá, C., Palau, G., Moltó, E., & Chueca, P. (2012). CFD
684 model of the effect of canopy on air velocity in air-assisted treatments in mandarin
685 orchards. In: Book of papers ISBN: 978-84-615-9928-8. *International Conference of*
686 *Agricultural Engineering CIGR-AgEng 2012*. Valencia (España), 8-12 July 2012.
687
688 Salcedo, R., Granell, R., Garcerá, C., Palau, G., Moltó, E., & Chueca, P. (2013).
689 Validation of a CFD model of the effect of an orange tree canopy on the air flow
690 produced by an air-blaster sprayer. In: E. Moltó et al. (eds.). Book of Abstracts. *12th*
691 *International Workshop on Sustainable Plant Protection Techniques in Fruit Growing*
692 *(SuproFruit2013)*. Valencia, Spain. p. 95-97.
693
694 Salcedo, R., Garcerá, C., Granell, R., Moltó, E., & Chueca, P. (2015a). Description of
695 the airflow produced by an air-assisted sprayer during pesticide applications to citrus.
696 *Spanish Journal of Agricultural Research*, 13, 2-8.
697
698 Salcedo, R., Granell, R., Palau, G., Vallet, A., Garcerá, C., Chueca, P., & Moltó, E.
699 (2015b). Design and validation of a 2D CFD model of the airflow produced by an
700 airblast sprayer during pesticide treatments of citrus. *Computers and Electronics in*
701 *Agriculture*, 116, 150-161.
702
703 Salyani, M., Farooq, M., & Sweeb, R. (2007). Spray deposition and mass balance in
704 citrus orchards applications. *Transactions of ASABE*, 50, 1963-1969.
705
706 Salyani, M., Miller, D.R., Farooq, M., & Sweeb, R.D. (2013). *Effects of sprayer*
707 *operating parameters on airborne drift from citrus air-carrier sprayers*. Agricultural
708 Engineering International: CIGR Journal, 15(1), 27-36.
709
710 SDTF (Spray Drift Task Force) (1997) A summary of airblast application studies.
711 Report. Macon, Mo (USA): Stewart Agricultural Research Services, Inc., 12 pp.
712
713 Steinke, W.E., & Yates, W.E. (1989). Modifying Gaussian models to obtain improved
714 drift predictions. *Transactions of ASAE*, 89, 1525.
715
716 Teske, M.E., Bird, S.L., Esterly, D.M., Curbishley, T.B., Ray, S.L. & Perry, S.P. (2002)
717 AgDrift: A model for estimating near-field spray drift from aerial applications.
718 *Environmental Toxicology Chemistry*, 21, 659-671.
719
720 Teske, M.E., Thistle, H.W., & Ice, G.G. (2003). Technical advances in modeling aerially
721 applied sprays. *Transactions of ASAE*, 46, 985-996.
722

Thompson, N., & Ley, A.J. (1983). Estimating spray drift using a random-walk model of evaporating drops. *Journal of Agricultural Engineering Research*, 28, 419-435.

Tsai, M.Y., Elgethun, K., Ramaprasad, J., Yost, M.G., Felsot, A.F., & Hebert, V.R. (2005). The Washington aerial spray drift study: modeling pesticide spray drift deposition from an aerial application. *Atmospheric Environment*, 39, 6194-6203

Versteeg, H.K., & Malalasekera, W. (1995). An introduction to Computational Fluid Dynamics. The Finite Volume Method. *Prentice Hall*, Upper Saddle River.

Xu, Z.G., Walklate, P.J., Rigby, S.G., & Richardson, G.M. (1998). Stochastic modelling of turbulent spray dispersion in the near-field of orchard sprayers. *Journal of Wind Engineering and Industrial Aerodynamic*, 74-76, 295-304.

Zhu, H., Reichard, D.L. Fox, R.D. Brazee, R.D., & Ozkan, H.E. (1994). Simulation of drift of discrete sizes of water droplets from field sprayers. *Transactions of the ASAE*, 37(5), 1401-1407.

Fig. 1. Experimental air velocities (i), with the vortices above and behind the target tree when the fan is facing it (Salcedo et al., 2015a). The streamlines (ii) resulting from the Eulerian CFD model reproduce the same structures (Salcedo et al., 2015b).

Fig. 2. Model computational domain.

Fig. 3. Inclination (°) for each nozzle referred to the horizontal axis (i) and sections through which droplets where introduced in the domain (ii).

Fig. 4. Wind velocity profile during the second part of the simulation

Fig. 5. Droplets position for instants t = 0.10 s (i), t = 0.20 s (ii) and t = 0.35 s (iii). The colour scale indicates the size of the droplets. Within each time the scale varies depending on the present droplets.

Fig. 6. Droplets position for instants t = 2.35 s (i), t = 5.35 s (ii), t = 8.35 s (iii), t = 11.35 s (iv) and t = 17.35 s (v). The colour scale indicates the size of the droplets. Within each time the scale varies depending on the present droplets.

Fig. 7. Location of droplets during the simulation.

Fig. 8. Maximum, minimum and mean distance to inlet A (m) of droplets from Cloud 1 (i) and Cloud 2 (ii) during the simulation.

Fig. 9. Maximum, minimum and mean height (m) of droplets from Cloud 1 (i) and Cloud 2 (ii) during the simulation.

Fig. 10. Maximum, minimum and mean velocity magnitude (m s^{-1}) of droplets from Cloud 1 (i) and Cloud 2 (ii) during the simulation.

Fig. 11. Maximum, minimum and mean Reynolds number (-) for droplets from Cloud 1 (i) and Cloud 2 (ii) during the simulation.

Fig. 12. Maximum, minimum and mean geometric diameter (μm) droplets from Cloud 1 (i) and Cloud 2 (ii) during the simulation

Fig. 13. Dv10, Dv50 and Dv90 (μm) from Cloud 1 (i) and Cloud 2 (ii) during the simulation.

803
804

Figure 9

Click here to download high resolution image

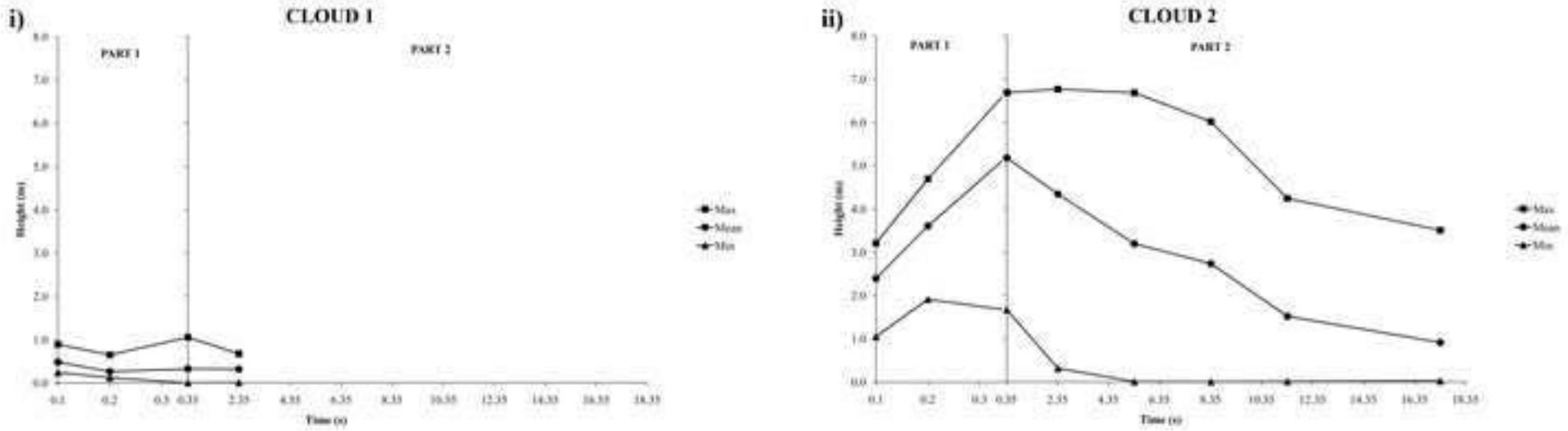

Figure 10

Click here to download high resolution image

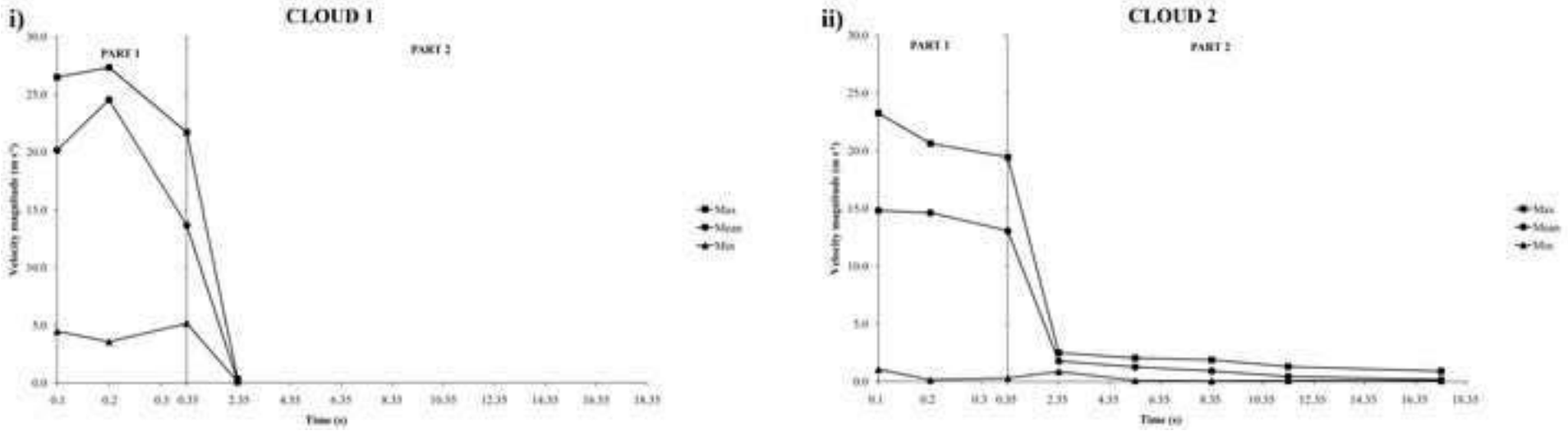

Figure 11

Click here to download high resolution image

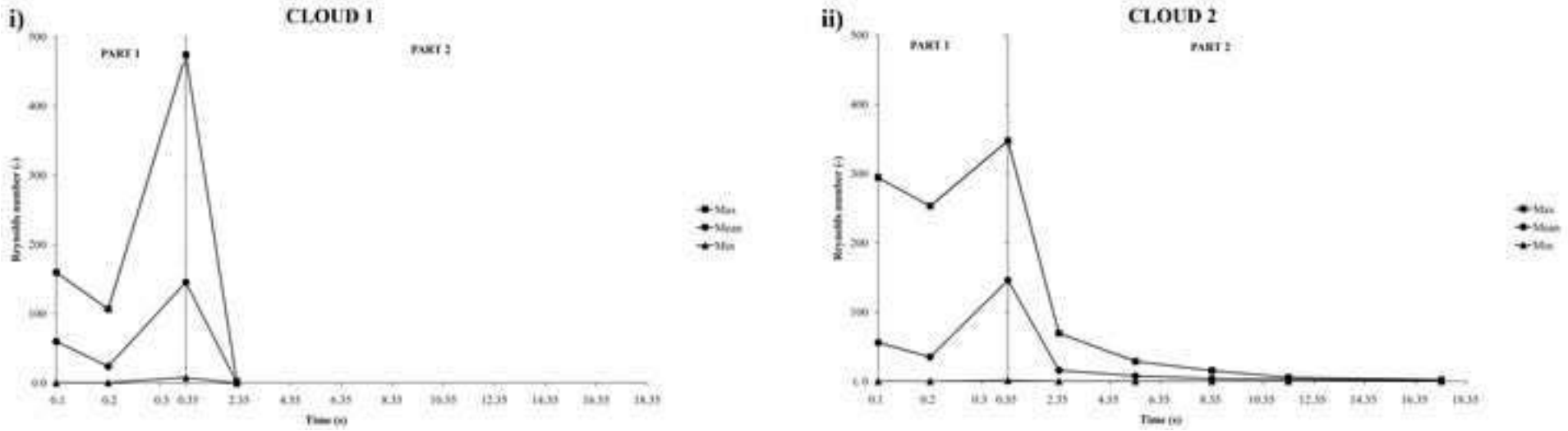

Figure 12

Click here to download high resolution image

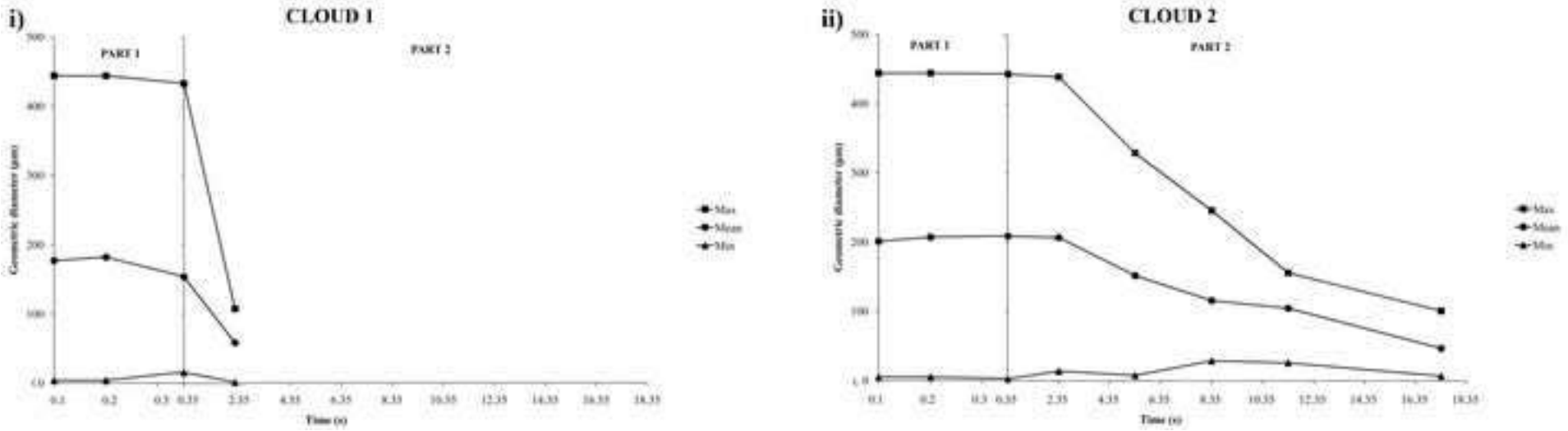

Figure 13

Click here to download high resolution image

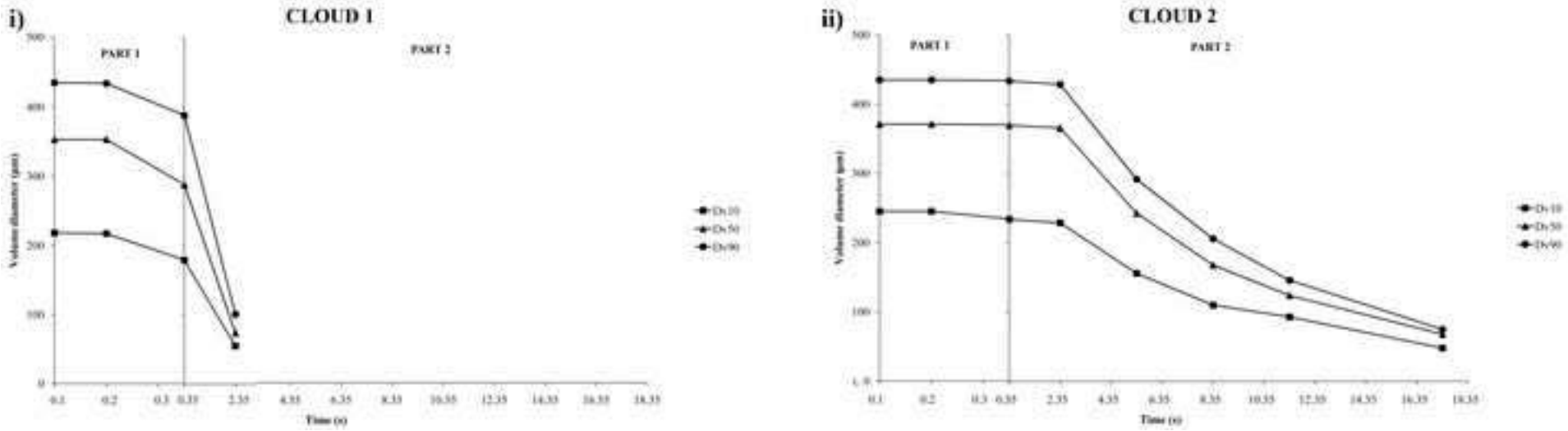

Figure 1

Click here to download high resolution image

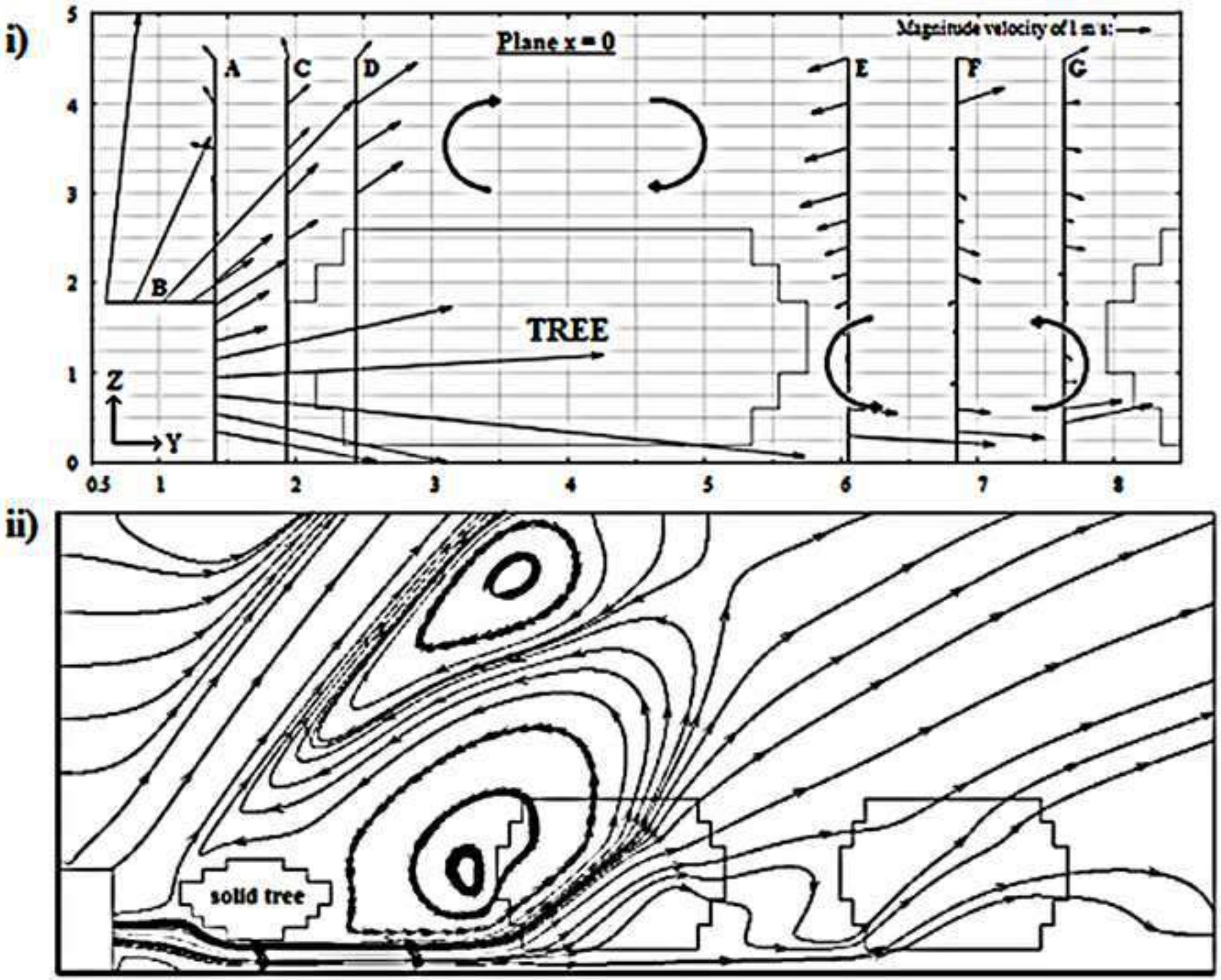

Figure 2

Click here to download high resolution image

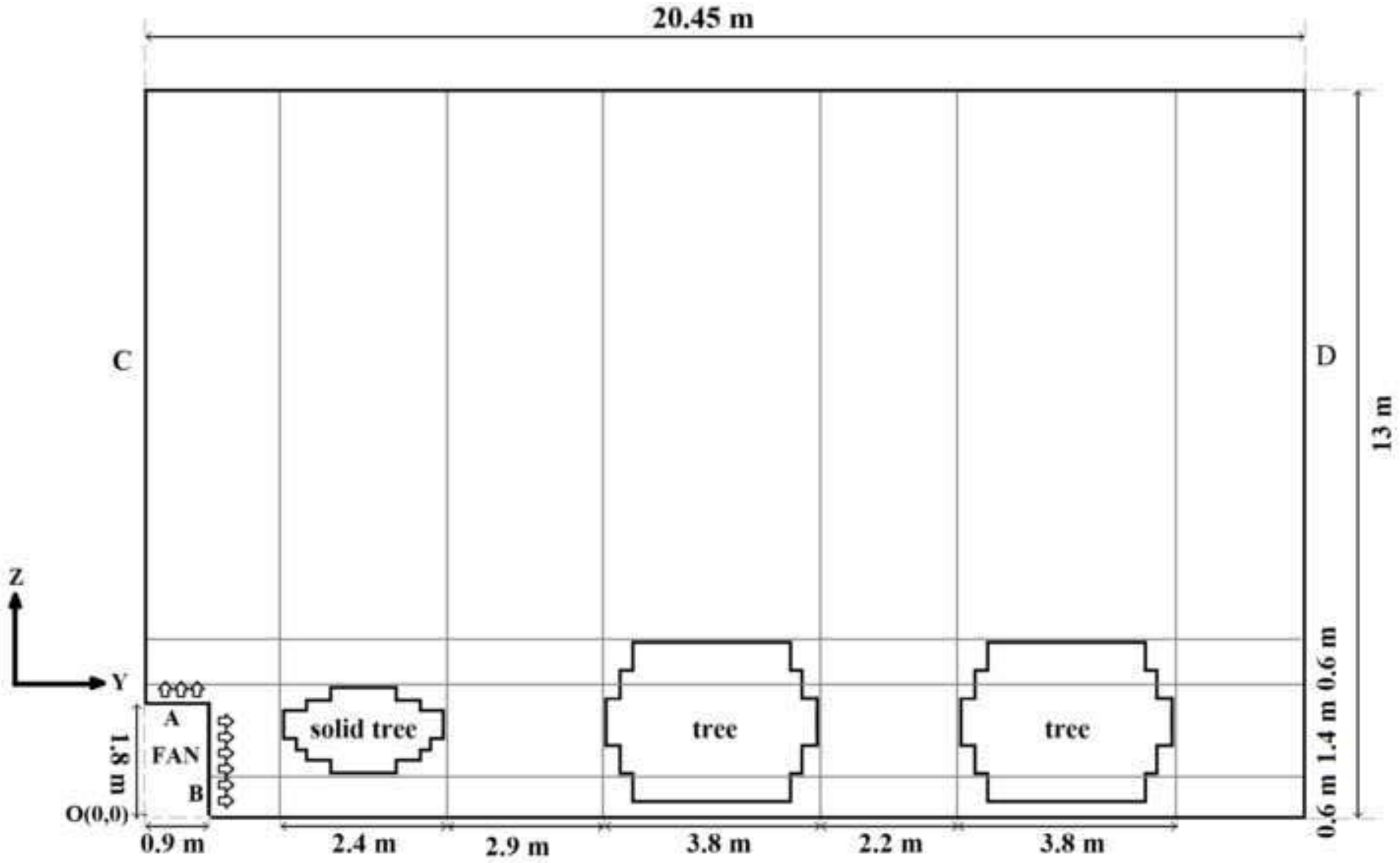

Figure 3

Click here to download high resolution image

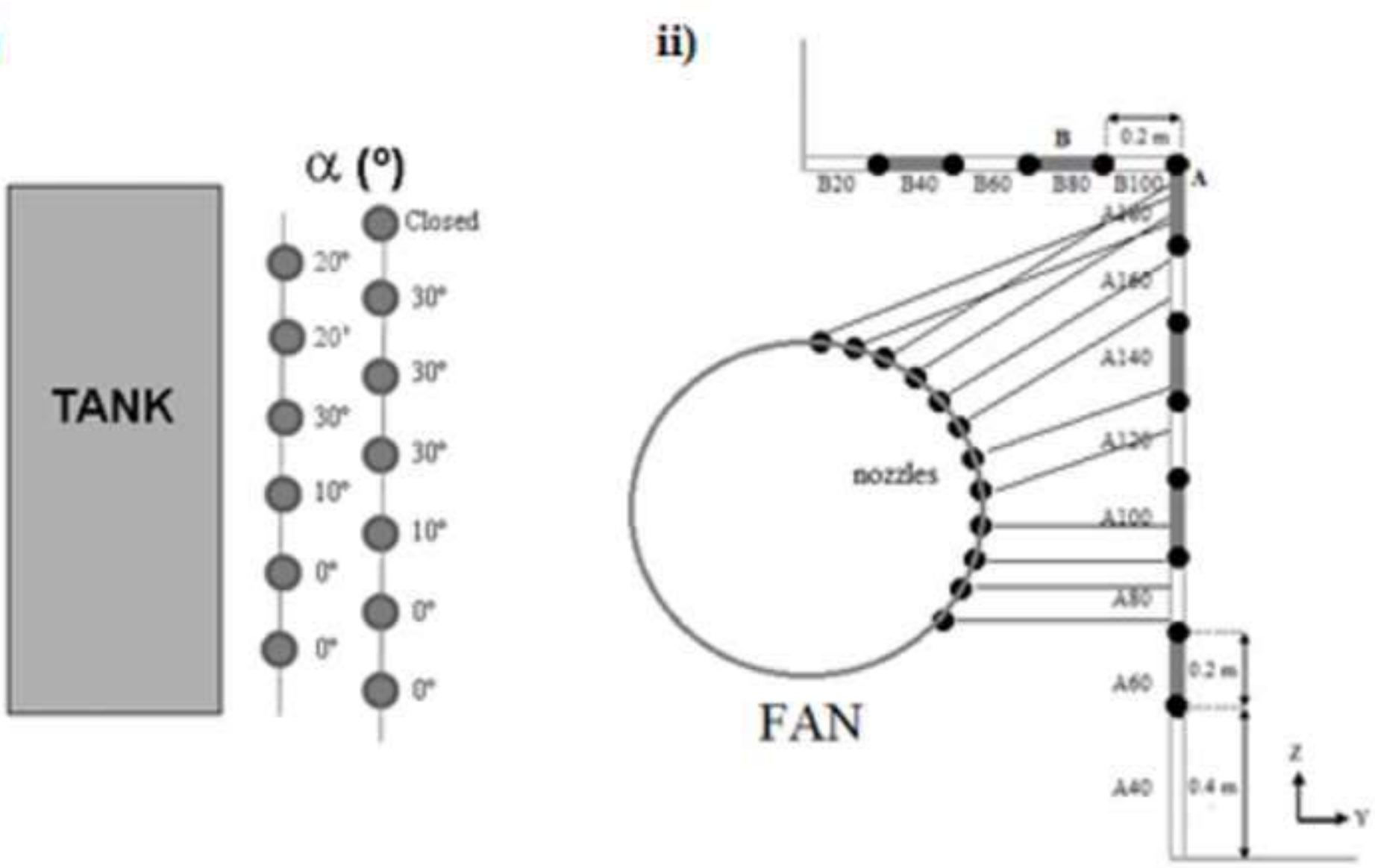

Figure 4

Click here to download high resolution image

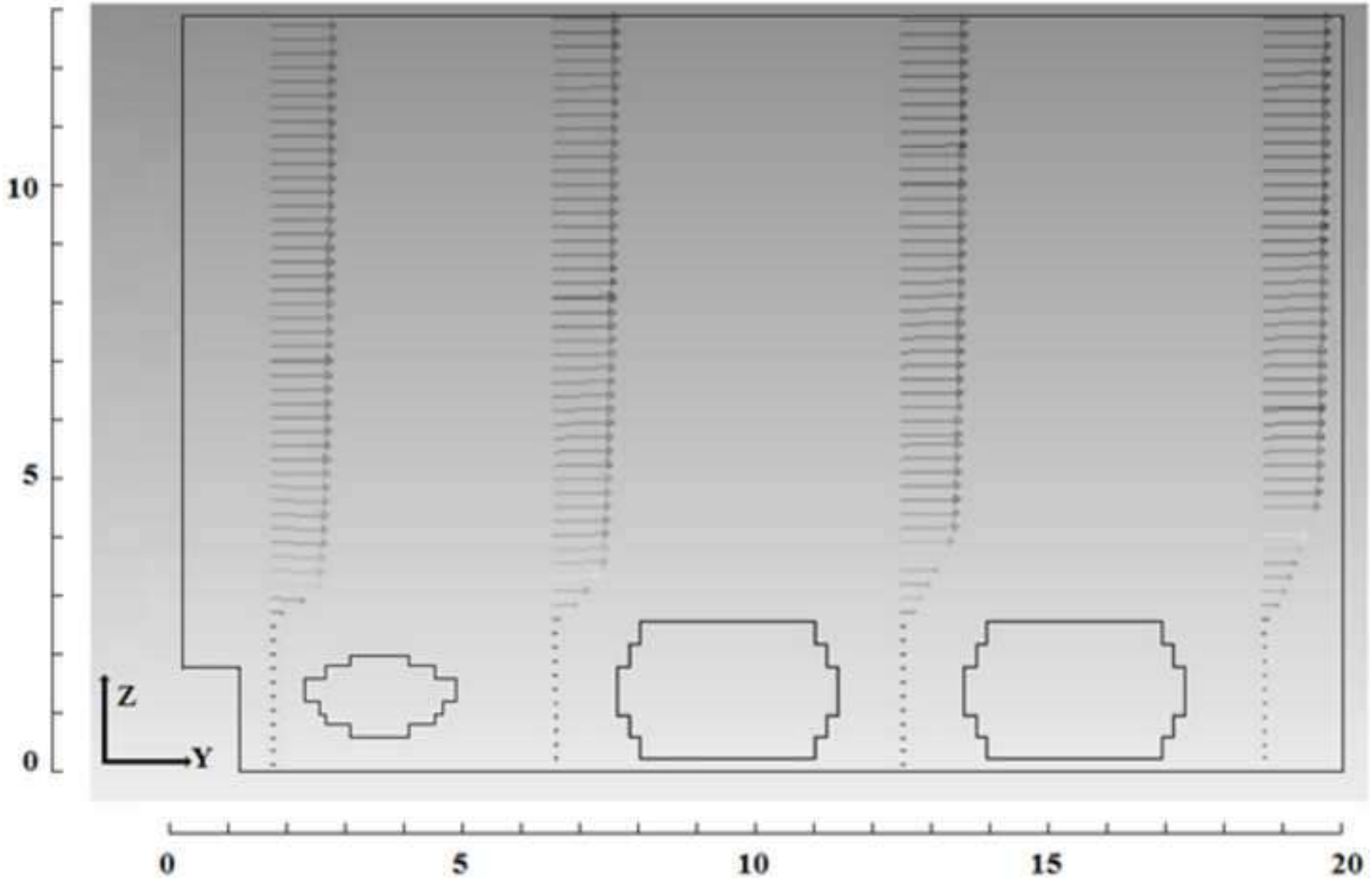

Figure 5

Click here to download high resolution image

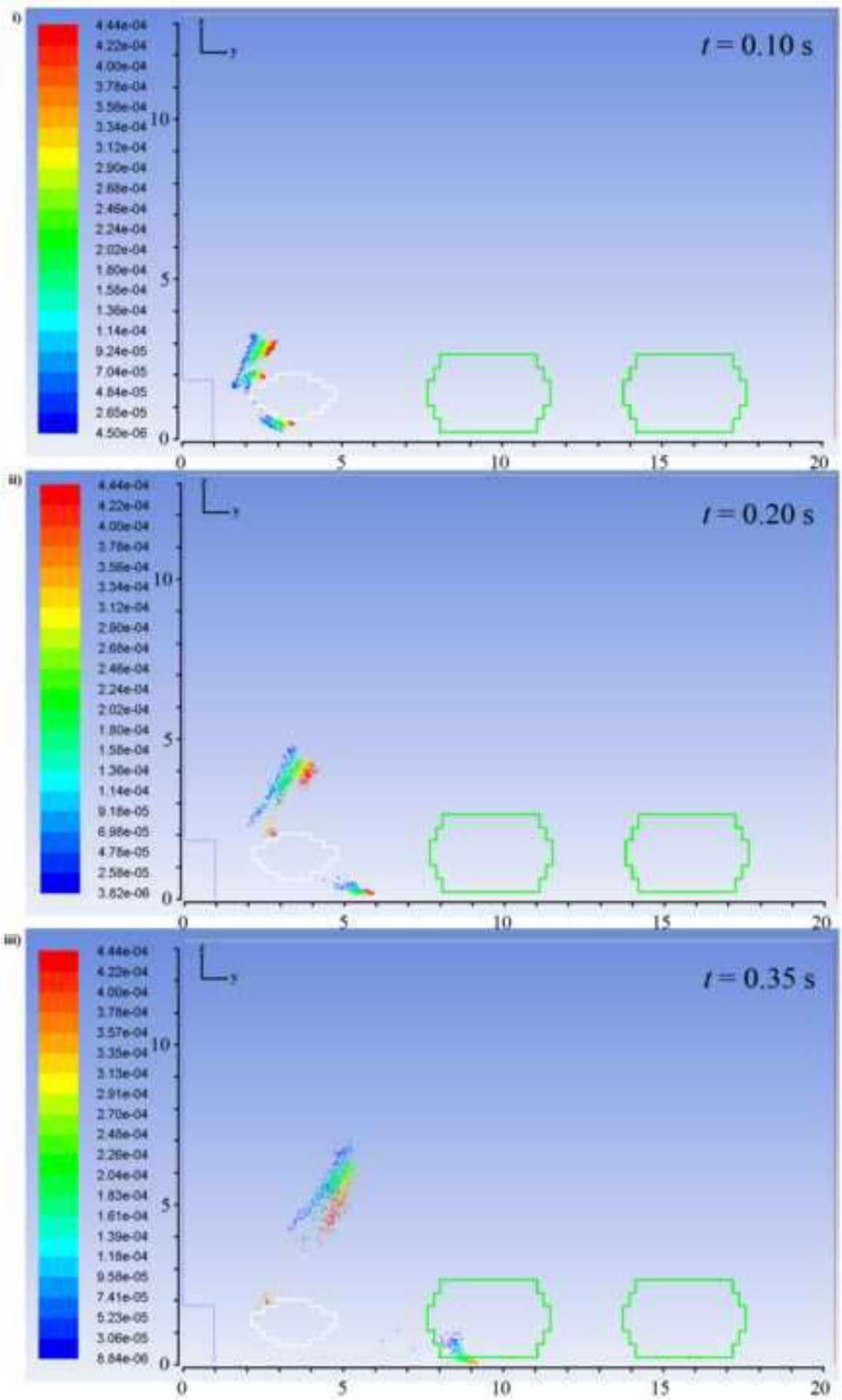

Figure 6

Click here to download high resolution image

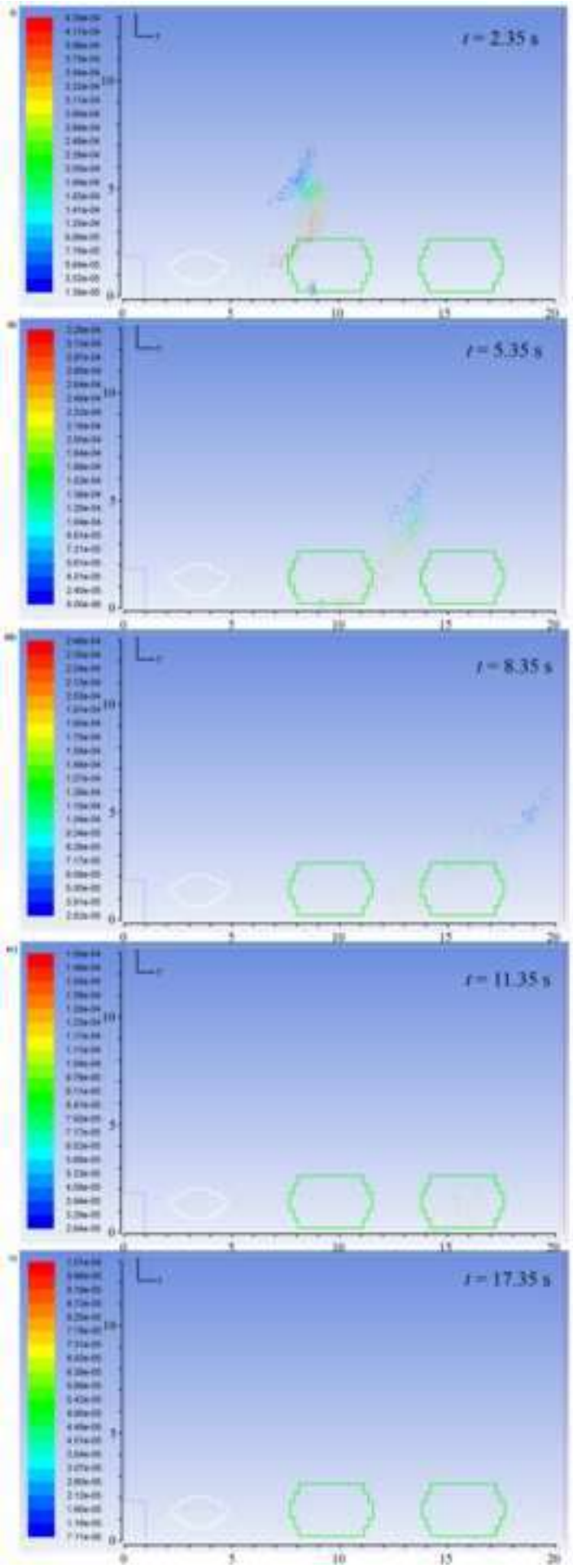

Figure 7

Click here to download high resolution image

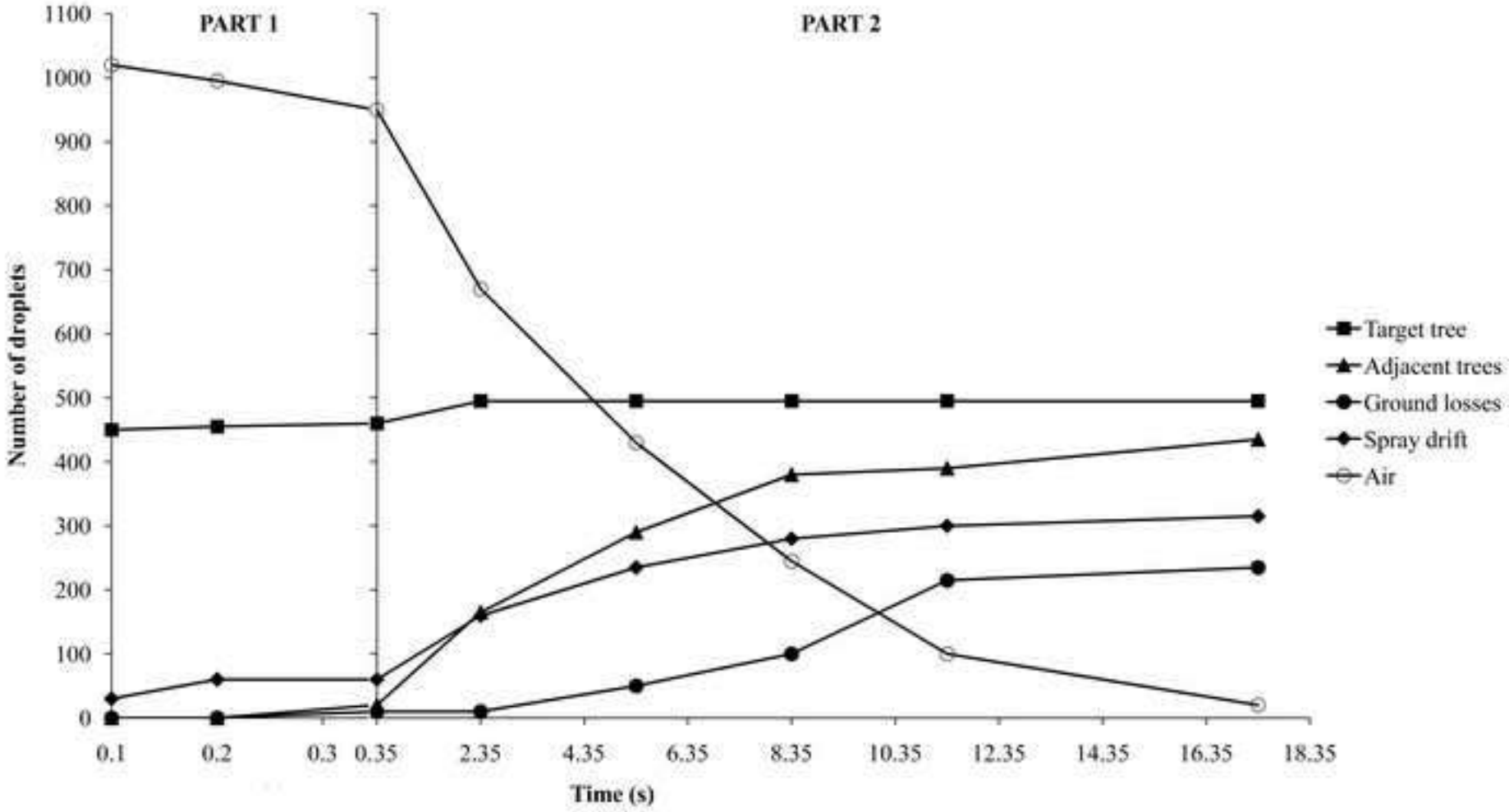

Figure 8

Click here to download high resolution image

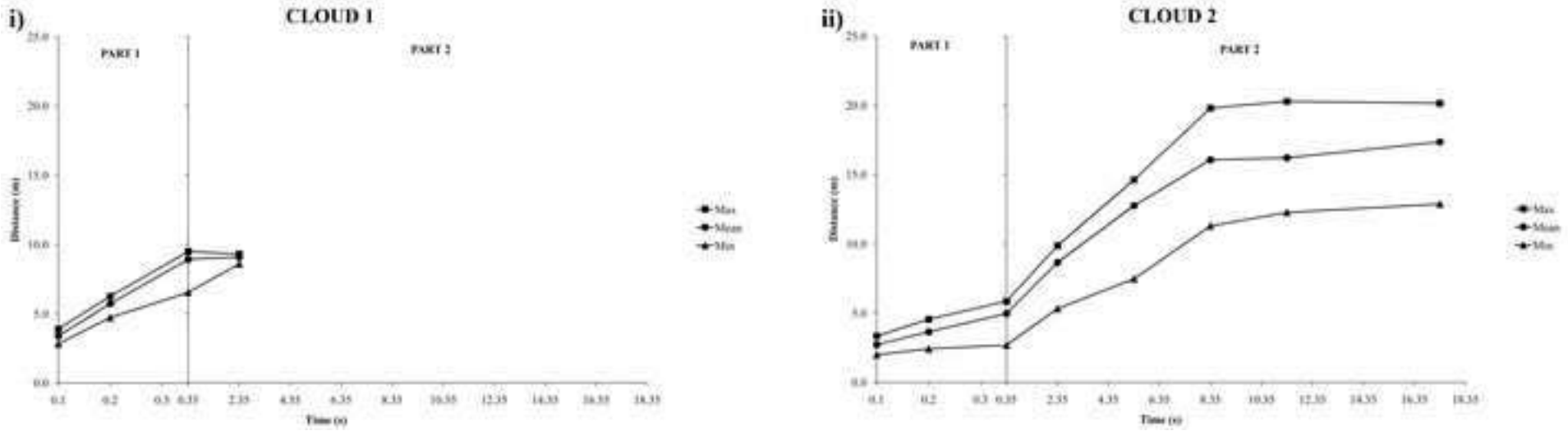

Tables

Table 1. Inlet velocity components (U_{fy}, U_{fz} (m s^{-1})) and turbulence intensities (I (%)) assigned to each section determined in field conditions (Salcedo et al., 2015b)

Section	U_{fy} (m s^{-1})	U_{fz} (m s^{-1})	I (%)
A40	1.1	0.1	50.0
A60	25.9	-4.8	4.0
A80	22.7	-3.2	6.1
A100	25.5	0.6	3.6
A120	18.9	3.2	12.6
A140	10.5	3.1	16.0
A160	13.2	6.4	13.6
A180	15.7	9.8	10.7
B20	10.4	2.7	22.9
B40	3.7	6.3	29.4
B60	7.2	9.2	16.8
B80	8.2	6.2	14.4
B100	13.8	9.5	8.2

Table 2. Values from the associated parameters to the dynamic behaviour in each cloud for different instants of the first part of the simulation: mass centre position to the inlet A (Y_m, Z_m (m)), components and magnitude velocity mass centre (U_{my}, U_{mz}, U_m (m s^{-1})), components and linear momentum magnitude (P_y, P_z, P (kg m s^{-1})) and total kinetic energy (E (J)).

	Cloud 1			Cloud 2		
	t = 0.10 s	t = 0.20 s	t = 0.35 s	t = 0.10 s	t = 0.20 s	t = 0.35 s
Y_m (m)	3.7	6.0	9.2	3.0	3.9	4.9
Z_m (m)	0.5	0.2	0.1	2.6	3.6	4.6
U_{my} (m s^{-1})	21.1	24.2	17.3	11.1	7.4	5.4
U_{mz} (m s^{-1})	-4.1	-1.8	-0.7	11.0	8.2	5.6
U_m (m s^{-1})	21.5	24.2	17.3	15.7	11.1	7.8
P_y (kg m s^{-1})	$4.1\cdot10^{-5}$	$4.5\cdot10^{-5}$	$1.6\cdot10^{-5}$	$8.2\cdot10^{-5}$	$5.5\cdot10^{-5}$	$3.9\cdot10^{-5}$
P_z (kg m s^{-1})	$-7.9\cdot10^{-6}$	$-3.4\cdot10^{-6}$	$-6.0\cdot10^{-7}$	$8.2\cdot10^{-5}$	$6.1\cdot10^{-5}$	$4.0\cdot10^{-5}$
P (kg m s^{-1})	$4.1\cdot10^{-5}$	$4.6\cdot10^{-5}$	$1.6\cdot10^{-5}$	$1.2\cdot10^{-4}$	$8.2\cdot10^{-5}$	$5.6\cdot10^{-5}$
E (J)	$4.5\cdot10^{-4}$	$5.6\cdot10^{-4}$	$1.4\cdot10^{-4}$	$9.8\cdot10^{-4}$	$5.5\cdot10^{-4}$	$3.2\cdot10^{-4}$

Table 3. Values from the associated parameters to the dynamic behaviour in each cloud for different instants of the second part of the simulation: mass centre position to the inlet A (Y_m, Z_m (m)), components and velocity mass centre magnitude (U_{my}, U_{mz}, U_m (m s^{-1})), components and linear momentum magnitude (P_y, P_z, P (kg m s^{-1})) and total kinetic energy (E (J)).

	Cloud 1	Cloud 2				
	t =2.35 s	t=2.35 s	t=5.35 s	t=8.35 s	t=11.35s	t=17.35 s
Y_m (m)	9.1	8.6	11.8	14.3	15.6	17.3
Z_m (m)	0.2	3.0	1.7	1.4	1.1	0.6
U_{my} (m s^{-1})	0.1	0.9	0.3	0.2	0.1	0.1
U_{mz} (m s^{-1})	-0.2	-1.4	-0.9	-0.5	-0.4	-0.1
U_m (m s^{-1})	0.2	1.7	0.9	0.6	0.4	0.2
P_y (kg m s^{-1})	$5.9\cdot10^{-10}$	$5.7\cdot10^{-6}$	$4.0\cdot10^{-7}$	$7.2\cdot10^{-8}$	$1.1\cdot10^{-8}$	$2.8\cdot10^{-10}$
P_z (kg m s^{-1})	$-1.1\cdot10^{-9}$	$-8.4\cdot10^{-6}$	$-1.2\cdot10^{-6}$	$-1.7\cdot10^{-7}$	$-2.8\cdot10^{-8}$	$-4.2\cdot10^{-10}$
P (kg m s^{-1})	$1.3\cdot10^{-9}$	$1.0\cdot10^{-5}$	$1.3\cdot10^{-6}$	$1.9\cdot10^{-7}$	$3.0\cdot10^{-8}$	$5.0\cdot10^{-10}$
E (J)	$1.5\cdot10^{-10}$	$1.0\cdot10^{-5}$	$8.0\cdot10^{-7}$	$8.2\cdot10^{-8}$	$8.3\cdot10^{-9}$	$6.5\cdot10^{-11}$

Table 4. Parameters associated to the kinetics droplet for each instant of the part 2 of the simulation and for droplets with at least 3.0 m height (Mean (standard error)): sedimentation velocity magnitude (U_s, m s^{-1}), relaxation time (τ, ms), relaxation time at sedimentation (τ_s, ms) and drag force (F_d, N).

	t = 0.35 s	t = 2.35 s	t = 5.35 s	t = 8.35 s	t = 11.35 s
U_s (m s^{-1})	0.73 (0.02)	0.61 (0.02)	0.30 (0.01)	0.16 (0.01)	0.18 (0.04)
τ (ms)	27 (1)	30 (1)	10 (2)	5 (1)	8 (2)
τ_s (ms)	74 (2)	62 (2)	30 (1)	16 (1)	19 (4)
F_d (N)	$2.6\cdot10^{-6}$ ($6.7\cdot10^{-8}$)	$3.1\cdot10^{-7}$ ($5.4\cdot10^{-9}$)	$2.7\cdot10^{-7}$ ($2.2\cdot10^{-8}$)	$2.1\cdot10^{-7}$ ($1.9\cdot10^{-8}$)	$4.6\cdot10^{-8}$ ($1.4\cdot10^{-8}$)

Table 5. Mean values of Sedimentation velocity magnitude U_s (m s^{-1}) and wind velocity U (m s^{-1}) every 0.5 m between 3 m and 7 m height.

Height (m)	Sedimentation velocity magnitude *Us* (m s^{-1})					
	t = 0.35 s	t = 2.35 s	t = 5.35 s	t = 8.35 s	t = 11.35 s	U wind (m s^{-1})
[3.0-3.5]	0.78	1.27	0.59	0.28	0.20	0.92
[3.5-4.0]	1.32	1.18	0.41	0.20	-	0.94
[4.0-4.5]	1.10	0.74	0.25	0.13	-	0.95
[4.5-5.0]	0.94	0.61	0.17	0.07*	-	0.97
[5.0-5.5]	0.71	0.37	0.10	0.05*	-	0.98
[5.5-6.0]	0.66	0.17	0.07*	0.03*	-	0.99
[6.0-6.5]	0.40	0.08*	0.04*	-	-	1.00
[6.5-7.0]	0.06*	0.04*	-	-	-	1.01

* Droplets susceptible to be dragged by the airflow and become atmospheric drift because U_s is lower than 10% of the wind velocity magnitude (Holterman (2003).

Table 6. Mean values for Relaxation time at sedimentation τ_s (ms) every 0.5 m between 3 m and 7 m height.

Height (m)	t = 0.35 s	t = 2.35 s	t = 5.35 s	t = 8.35 s	t = 11.35 s
[3.0-3.5]	79	130	61	28	20
[3.5-4.0]	135	120	42	20	-
[4.0-4.5]	112	76	26	13	-
[4.5-5.0]	96	62	17	7	-
[5.0-5.5]	72	37	10	6	-
[5.5-6.0]	67	18	7	3	-
[6.0-6.5]	41	8	4	-	-
[6.5-7.0]	6	4	-	-	-

Table 7. Mean values of Evaporation rate k_0 (μm^2 s^{-1}) every 0.5 m between 3 m and 7 m height.

Height (m)	t = 0.35 s	t = 2.35 s	t = 5.35 s	t = 8.35 s	t = 11.35 s
[3.0-3.5]	597	625	587	573	569
[3.5-4.0]	628	620	579	569	-
[4.0-4.5]	616	596	571	564	-
[4.5-5.0]	607	589	567	560	-
[5.0-5.5]	595	576	562	559	-
[5.5-6.0]	591	566	560	556	-
[6.0-6.5]	578	560	558	-	-
[6.5-7.0]	558	556	-	-	-

Table 8. Comparison of the percentages from the applied volume between experiment performed by Chueca, Moltó and Garcerá (2011) and simulation.

	Experiment (%)	Simulation (%)
Targeted vegetation	43	44
Adjacent trees	5	28
Ground	25	20
Atmospheric drift	18	8
Not found	13	-